

RSC Advances



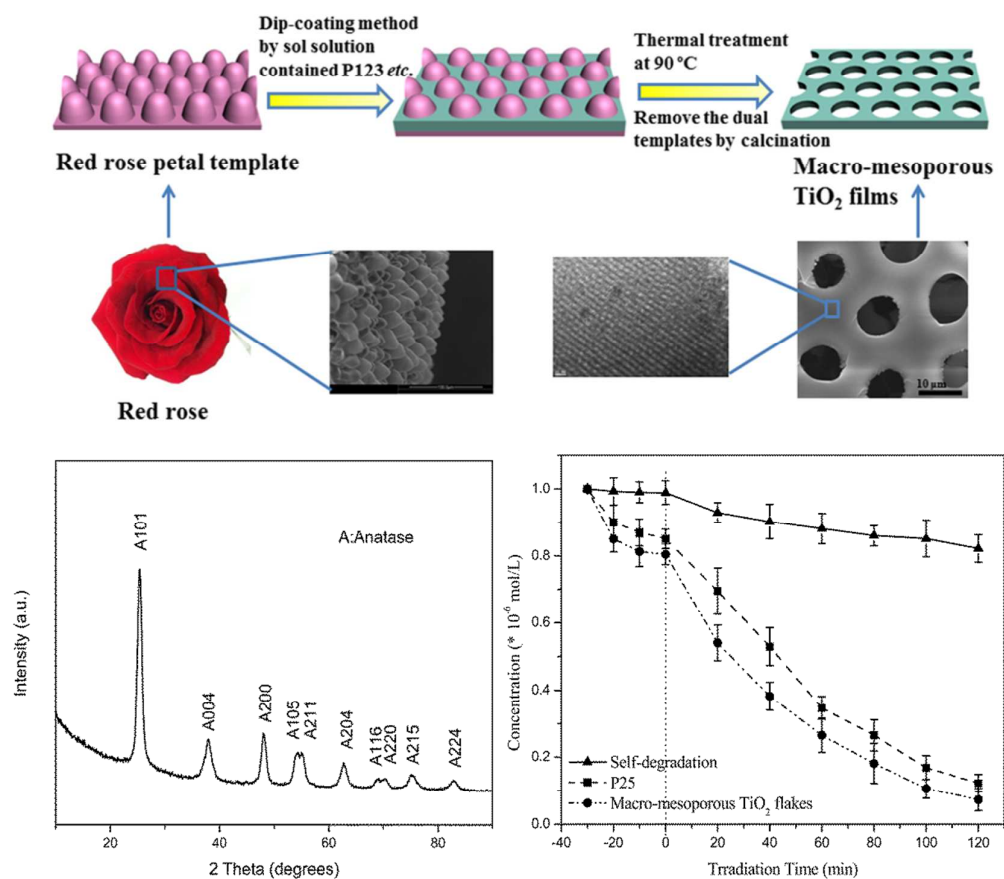
This is an *Accepted Manuscript*, which has been through the Royal Society of Chemistry peer review process and has been accepted for publication.

Accepted Manuscripts are published online shortly after acceptance, before technical editing, formatting and proof reading. Using this free service, authors can make their results available to the community, in citable form, before we publish the edited article. This *Accepted Manuscript* will be replaced by the edited, formatted and paginated article as soon as this is available.

You can find more information about *Accepted Manuscripts* in the [Information for Authors](#).

Please note that technical editing may introduce minor changes to the text and/or graphics, which may alter content. The journal's standard [Terms & Conditions](#) and the [Ethical guidelines](#) still apply. In no event shall the Royal Society of Chemistry be held responsible for any errors or omissions in this *Accepted Manuscript* or any consequences arising from the use of any information it contains.

Graphical abstract:



Textual abstract:

Hierarchically ordered macro-mesoporous anatase TiO₂ flakes were synthesized by using rose petals and P123 as dual templates with high photocatalytic activity.

ARTICLE

Bio-templated synthesis of hierarchically ordered macro-mesoporous anatase titanium dioxide flakes with high photocatalytic activity

Cite this DOI:
10.1039/x0xx00000x

Received 00th January 2012,
Accepted 00th January 2012

DOI: 10.1039/x0xx00000x

www.rsc.org/

Bing Li,^a Jianquan Zhao,^c Jing Liu,^a Xinyu Shen,^a Shaobo Mo^{a*} and Hua Tong^{ab**}

Highly ordered macro-mesoporous anatase titanium dioxide (TiO₂) flakes were synthesized by sol-gel method in an acidic medium, using fresh natural rose (*Rosa hybrida* L.) petals and triblock copolymer P123 (EO₂₀PO₇₀EO₂₀) as dual templates. The resulting flakes were characterized by Raman spectroscopy, X-ray diffraction (XRD), scanning electron microscopy (SEM), transmission electron microscopy (TEM) and nitrogen adsorption-desorption analysis. The results reveal that the bimodal porous material is in anatase phase, and the three-dimensionally ordered macroporous walls are composed of highly ordered mesopores. The Brunauer-Emmett-Teller (BET) surface area and the average size of mesopores are 125.91 m² g⁻¹ and 4.79 nm, respectively. The photocatalytic activity of the porous TiO₂ flakes was evaluated by photodegradation of Rhodamine B (RhB) under ultraviolet (UV) light. The obtained TiO₂ flakes exhibited a slightly higher photocatalytic activity than commercial photocatalyst Degussa P25.

Introduction

In recent years, many efforts have been devoted to the synthesis, characterization and application of bimodal macro-mesoporous materials,¹⁻⁶ due to organized pore networks and hierarchically multimodal pore-size distributions. For instance in catalysis, mesopores of them help impart a high surface-to-volume, providing numerous active sites and a substantial interfacial area for carrying out catalytic reaction while macropores favor great transportation of matter, offsetting transport limitations present in purely mesoporous materials especially in viscous systems of for large molecules (e.g., polymers, biomolecules).^{1,2}

⁷ Porous objects with nm- or μm-scale features and discrete particles can be used as templates to synthesize periodic macropores, and ordered mesoporous materials have been fabricated by using surfactants and amphiphilic copolymers.^{8,9} Among these commonly used artificial macroporous templates such as polystyrene^{1,5,6} and silica microspheres¹⁰, there were some disadvantages of high cost, complicated procedure of preprocessing and removing, which limited their applications in synthesis of macroporous materials. Relatively, natural organisms with unique multi-level structure and morphology can be used to provide porous biotemplate in the preparation of hierarchical materials because of their advantages such as low cost, environment-friendly and widely distributed.¹¹⁻¹³

Currently, hybrid tea varieties of *Rosa hybrida* L. (rose) are among the most important cash crops in the floriculture industry.¹⁴ The close arrays of micropapillae and the microgrooves can be observed on the surface of fresh natural rose petals.¹⁵ The noteworthy is that the especial microstructures can provide macroporous template to the preparation of porous materials. When synthesis of materials occurs in the microgrooves without flooding the top of micropapillae, ordered macroporous structure will be obtained after removing the rose petals. And the fresh natural rose petals without any pretreatment as macroporous template can be easily removed during calcination. In addition, red roses that mean love are widely available and low cost, indicating that red roses as macroporous biotemplate can be widely used in the preparation of hierarchical porous materials.

TiO₂, possessing several favorable properties such as low cost, easy handling, nontoxicity, and resistance to photochemical and chemical erosion, has been widely applied in chemical sensor,¹⁶ solar cell,^{17,18} water splitting,^{4,19} environmental purification application²⁰ and other applications.^{21,22} As one of the main features of TiO₂, the photocatalytic activity is largely affected by crystal properties, porous properties and specific surface area.⁶ Among three crystalline phases of TiO₂, anatase phase has the highest photocatalytic and photoelectrochemical conversion activity

than those of rutile and brookite TiO_2 .²³⁻²⁵ In addition, the porous structure of TiO_2 is conducive to pollutant access, adsorption and decomposition, because many active sites provided by a large surface area are able to absorb large amounts of substances.^{25, 26} Meanwhile, macroporous channels existed in macro-mesoporous titania could serve as light propagation paths to improve the light utilization efficiency effectively in photocatalysis.^{27, 28}

With the rapid development of modern industry, disposal of water pollution has become more and more important. As a result of inadequate cleaning and processing technology in the printing and dyeing industry, about 10-20% of the dyes are retained in the wastewater with the features of complex components, high color and non-biodegradation.^{29, 30} Many dyes in wastewater are toxic, carcinogenic, mutagenic and degradation-resistant and must be removed, such as rhodamine B (RhB).³¹ Therefore, semiconducting titania materials have been currently paid much attention due to their marked photocatalytic effect in removing dye pollutants from wastewater; and RhB was commonly selected as photodegradable reactant via N-de-ethylation process to characterize the photocatalytic activity of TiO_2 samples and demonstrate the potential applicability of them in the disposal of printing and dyeing wastewater.^{30, 32-35}

In this work, macro-mesoporous anatase TiO_2 sample was synthesized by using natural rose petals, a new macroporous biotemplate, and P123 as dual templates via a sol-gel reaction. In the synthetic process, P123 was employed as the mesoporous structure-directing agent, while inexpensive and environment-friendly rose petals were used as an ideal biotemplate for the fabrication of laminar macroporous structure. The dual templates were both removed by calcination with the formation of anatase TiO_2 . The obtained TiO_2 flakes in the present method showed a slightly higher photocatalytic activity than that of commercial catalyst Degussa P25 on the degradation of RhB in the air.

Experimental section

Materials

Triblock copolymer Pluronic P123 (molecular weight, $M_w = 5800$, $\text{EO}_{20}\text{PO}_{70}\text{EO}_{20}$) was purchased from Aldrich. P25 was obtained from Guangzhou Hualisen Trade Co., Ltd. (Guangzhou, China). Tetrabutyl titanate ($\text{Ti}(\text{OC}_4\text{H}_9)_4$), acetylacetone ($\text{CH}_2(\text{COCH}_3)_2$), hydrochloric acid (HCl), ethanol (EtOH) and RhB were purchased from Sinopharm Chemical Reagent Co., Ltd. (Shanghai, China). All chemicals were of analytical grade and were used as received without further purification. Ultrapure water (18.2 M Ω) was obtained from a Milli-Q water system. The origin of *Rosa hybrida* L. (red rose) is Chenggong County, Kunming City, Yunnan Province.

Preparation

TiO_2 flakes were prepared by a modified method reported in paper.³⁶ At room temperature, P123 (1.5 g) was dissolved in a mixed solution containing HCl (1.6 ml), EtOH (15 ml) and ultrapure water (0.2 ml), under vigorous stirring for 1 h. Then, acetylacetone (0.2 ml) was added into the above transparent solution with stirring for 20 min and Tetrabutyl titanate (7.2 g) was added in the solution and the mixture was gently stirred in a sealed bottle at room temperature for 24 h. The TiO_2 sample was prepared by the dip-coating method. The fresh natural rose petals were immersed into the resulting sol solution and held for 20 s to let the TiO_2 precursor evenly cover the surface of natural rose petal biotemplate. The dip-coated sample was dried at room temperature for 7 days with 70-75% relative humidity (RH). Then the dry sample was submitted to thermal treatment at 90 °C for 24 h to consolidate the inorganic network. After that, it was calcined at 450 °C for 3 h in air at a heating rate of about 1 °C min⁻¹ to remove the dual templates. With the above process, the TiO_2 flakes were obtained.

Characterization

A Raman spectrum was recorded on a Raman microspectrometer (LabRam HR800, Jobin Yvon, France) with the 632.8 nm line of a He-Ne laser as excitation source. X-ray diffraction (XRD) pattern was collected on an X-ray diffractometer (D/max-A, Rigaku, Japan). Acquisition conditions were $\text{CuK}\alpha$ radiation ($\lambda = 1.5406 \text{ \AA}$) operated at 40 kV and 50 mA, a step size of 0.05° s⁻¹ and the scattering angles (2θ) ranging from 10° to 90°. Morphological investigations were carried out by using an environmental scanning electron microscope (Quanta200, FEI, Netherlands) and two transmission electron microscopes (Tecnai G2, FEI, Netherlands and 2010FEF, JOEL, Japan). Nitrogen adsorption-desorption isotherm was determined on a Micromeritics Tristar 3000 system (USA) at 77 K, with samples being heated at 180 °C in a vacuum prior to the measurements. BET method was utilized to calculate their surface areas and the pore-size distributions were derived from the desorption branches of isotherms based on Barrett-Joyner-Halenda (BJH) model.

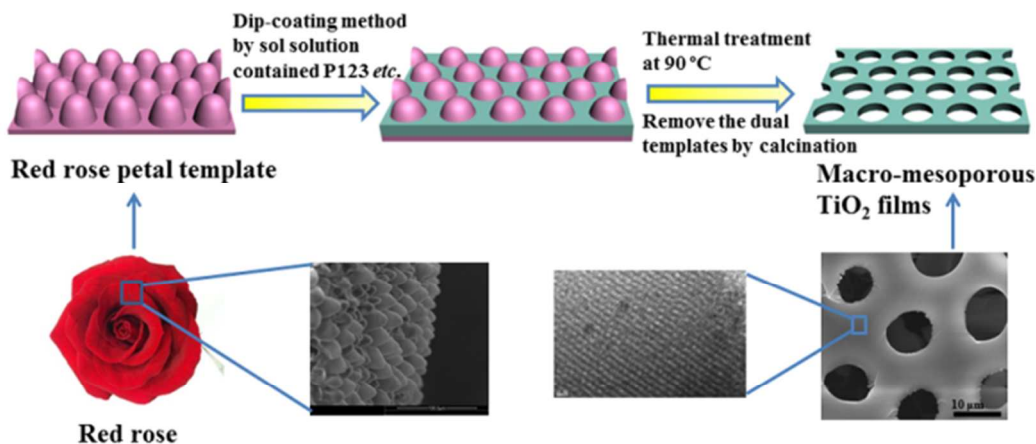
Photocatalytic activity

The photocatalytic activity of the obtained TiO_2 flakes was investigated by photodegradation of RhB under UV-light irradiation at ambient temperature and pressure. The UV source was a 250 W Hg lamp with a maximum emission at approximately 365 nm. The lamp was placed 30 cm above the RhB solution and was kept cool by a recirculating water jacket (Pyrex). Briefly, the TiO_2 sample (0.01 g) was dispersed in RhB dye solution (80 ml, $C_0 = 1 \times 10^{-5} \text{ M}$, pH 6.0) in ultrasonication. The suspension was then magnetically stirred in the dark for 30 min until an adsorption-desorption equilibrium between the catalyst surface and the dye was reached, and then the reaction mixture was exposed to the UV light with continuous magnetic stirring. The suspension (5 ml) was taken during the dark adsorption process and the illumination period (10 min and 20 min, respectively) and then centrifuged to

remove the catalysts to analyze the amount of RhB remaining in the solution. The ultraviolet-visible (UV-Vis) adsorption spectra of the taken solutions were obtained by a Shimadzu UV-2550 UV-Vis scanning spectrophotometer at $\lambda_{\text{max}} = 554 \text{ nm}$. In addition, a control experiment using commercial photocatalyst Degussa P25 and a blank experiment (self-

photosensitized process) were also measured under the identical experimental conditions.

Results and discussion



Scheme 1 Schematic representation of the highly ordered macro-mesoporous anatase TiO_2 flakes

The general preparation of highly ordered macro-mesoporous TiO_2 flakes can be briefly described by the following process, as shown in Scheme 1. The fresh natural rose petals without any pretreatment were provided macroporous template for the synthesis of ordered macro-mesoporous TiO_2 flakes. Wherefore, when the fresh rose petals were dipped into the sol containing triblock copolymer P123 and TiO_2 precursor, the arrayed micropapillae were covered uniformly by precursor with high adhesive affinity to water. Due to gravity, the precursor flowed slowly from the top of micropapillae to microgrooves, while the organic-organic self-assembly of the TiO_2 precursor and triblock copolymer P123 occurred during the evaporation of volatile species at room temperature for 7 days with 70-75% RH, followed by thermosetting at 100°C and removing the dual templates by calcination. The ordered macro-mesoporous anatase TiO_2 flakes were consequently obtained. The detailed preparation process can be found in the experimental section.

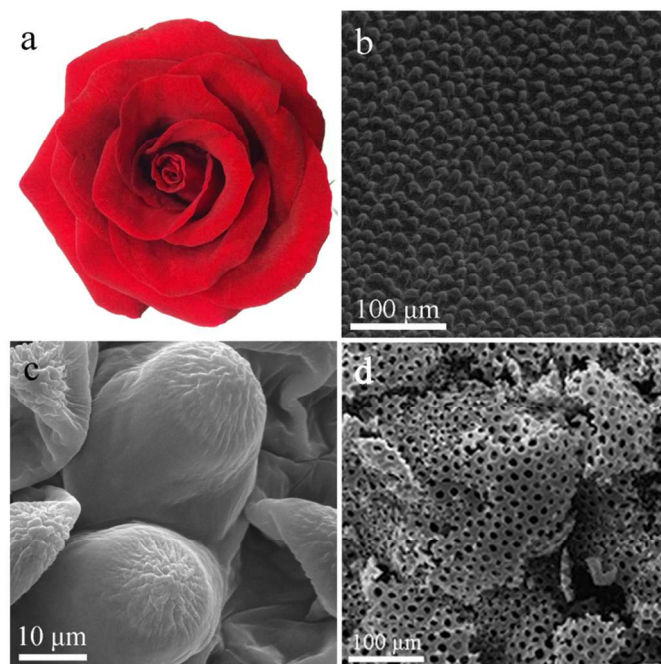


Fig. 1 (a-c) Correspond the fresh natural rose petal: (a) is the photograph; (b) and (c) are the top-view and side-view SEM images of the natural rose petal without any pretreatment, respectively; (d) is the SEM image of the obtained TiO_2 flakes.

Fig. 1 shows the photograph and scanning electron microscopy (SEM) images of the fresh natural rose petal and SEM image of the obtained TiO_2 flakes. From the SEM images (Fig. 1b and c), a close array of micropapillae with 15-18 μm and many nanofolds existed on each papilla top are observed.

Meanwhile, some micropapillae collapsed in the vacuum environment of obtaining SEM images. A phenomenon of “petal effect” was observed by Feng et al.¹⁵ that these hierarchical micro- and nanostructures of rose petals provided sufficient roughness for superhydrophobicity but had high adhesive force with water. Therefore the sol containing triblock copolymer P123 and TiO₂ precursor could be flowed slowly from the top of micropapillae to microgrooves among micropapillae because of “petal effect”. It suggested that the especial microstructures without any pretreatment could be used to provide macroporous template in the preparation of hierarchical porous materials. As can be seen from the SEM image (Fig. 1d), the morphologies of the TiO₂ flakes exhibit lamellar array of macroporous structures determined by the ordered structure of natural rose petal template. Besides, the pore size of the macroporous and the thickness of lamellar structures are about 9.5 and 6.1 μm, respectively. The SEM results proved effectively that the fresh natural rose petals as a macroporous biotemplate were available for synthesis of ordered macroporous materials.

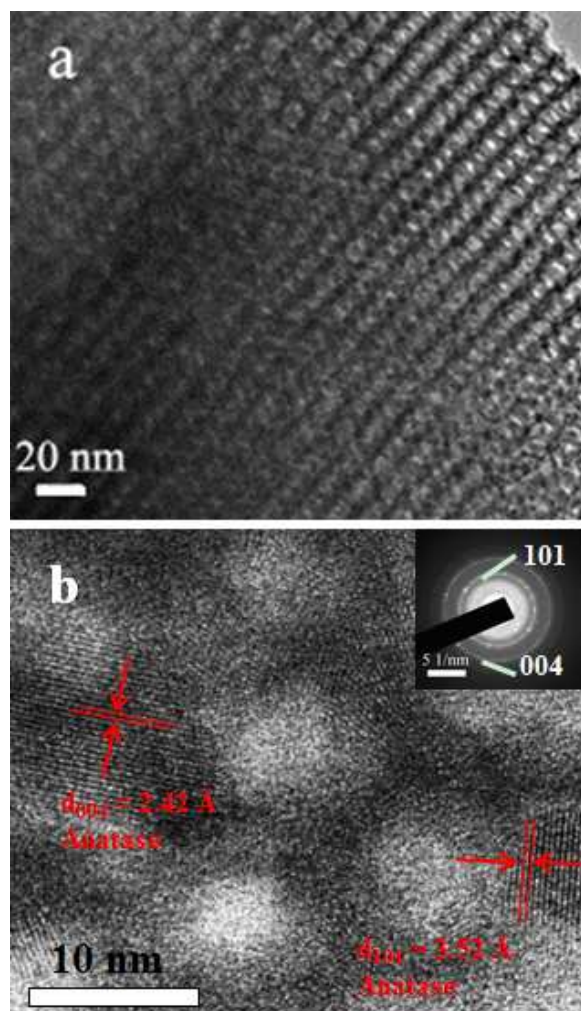


Fig. 2 TEM image (a) and high-resolution TEM (HRTEM) image (b) of the ordered macro-mesoporous TiO₂ flakes; the

inset in (b) shows selected-area electron diffraction (SAED) pattern.

TEM image of the ordered macro-mesoporous TiO₂ flakes are shown in Fig. 2a. The ordered macropores are uniform and the pore size was around 10 μm as suggested by the SEM image. Moreover, it also shows that the walls of these uniform macropores were made of highly ordered mesopores with hole and layer structures. The high-resolution TEM (HRTEM) image of the TiO₂ sample (Fig. 2b) clearly reveals that the mesoporous walls were composed of TiO₂ anatase nanoparticles. The mean crystallite size of the anatase nanoparticles measured from HRTEM image was ~9.8 nm. Moreover, some of the large TiO₂ nanoparticles even thrust into the channels and blocked the mesopores, indicating the formation of ink-bottle pores, which is further confirmed by the nitrogen adsorption-desorption isotherm. The mesoporous size and the wall thickness of the sample are estimated to be around 4.8 nm and 4.5 nm, respectively. It also shows clear lattice fringes, and the fringes of around 3.52 and 2.42 Å match well with the crystallographic spacings of the (101) and (004) planes of anatase phase, respectively. This observation confirms that the crystalline form of the highly crystalline TiO₂ nanoparticles was anatase phase. From the selected-area electron diffraction (SAED) pattern recorded on TiO₂ flakes (Fig. 2b, inset), a sequence of diffraction rings can be clearly observed, which is consistent with the polycrystalline anatase structure (JCPDS, No. 21-1272). It further confirms that the mesoporous walls of the obtained macro-mesoporous TiO₂ flakes were indeed made up of highly crystalline TiO₂ anatase nanoparticles.

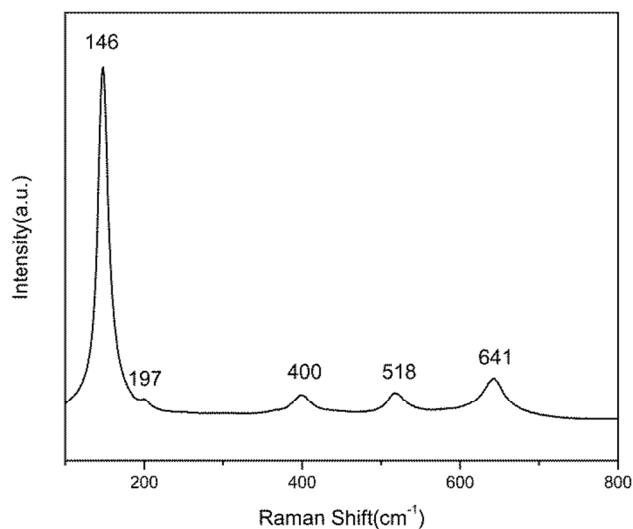


Fig. 3 Raman spectrum of the ordered macro-mesoporous TiO₂ flakes.

The crystallization of the ordered macro-mesoporous TiO₂ flakes was further studied by using Raman spectroscopy and XRD. As plotted in Raman spectrum (Fig. 3), the five bands located at 146, 197, 400, 518 and 641 cm⁻¹ are assigned to the five fundamental vibrational modes of anatase TiO₂ with the symmetries of E_g , E_g , B_{1g} , ($A_{1g} + B_{1g}$), E_g , respectively.^{37, 38} Accordingly, the XRD pattern (Fig. 4) exhibits eight diffraction

peaks, which are the typical peaks of indeed anatase (JCPDS, No. 21-1272). The results indicated a formation of TiO_2 nanocrystals after calcination at 450°C . Meanwhile, the average crystallite size calculated by the Scherrer formula using the (101) peak of anatase was 9.5 nm for the obtained TiO_2 flakes. The small size of the crystal grains could be helpful to the stabilization of anatase phase. The above-mentioned results reveal that the frameworks of the macro-mesoporous TiO_2 flakes were composed of anatase crystallite, which is consistent with the investigation of the TEM images.

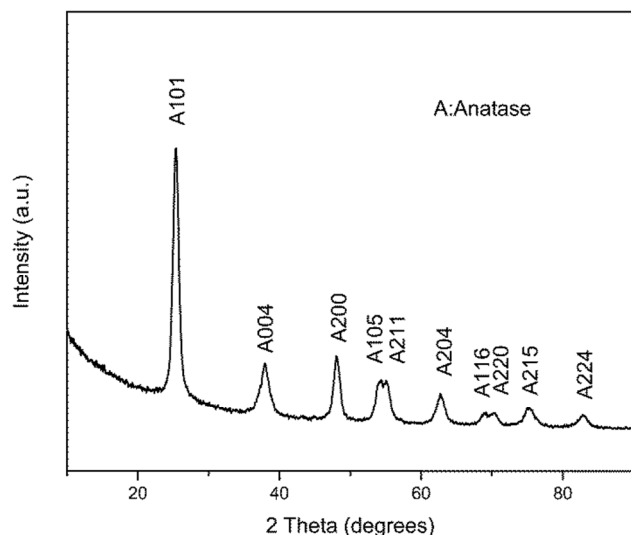


Fig. 4 XRD pattern of the ordered macro-mesoporous TiO_2 flakes.

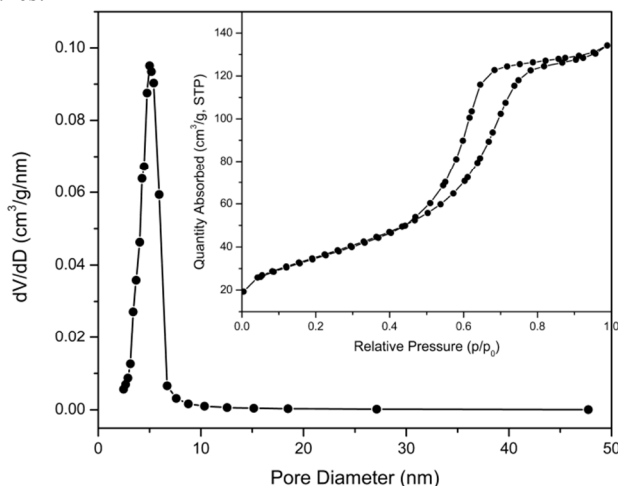


Fig. 5 Nitrogen adsorption-desorption isotherms (inset) and BJH pore-size distribution curves of the ordered macro-mesoporous TiO_2 flakes.

To detect the physico-chemical adsorption properties and pore parameters of TiO_2 flakes, the nitrogen adsorption-desorption isotherm and corresponding pore size distribution curve were investigated in detail. The isotherm of the TiO_2 films (Fig. 5, inset) is of classical type IV with the type H2 hysteresis loops at a relative pressure (P/P_0) range of 0.45-0.90. According to the IUPAC classification, the present isotherm

can be recognized as the characteristic curve of mesoporous materials with narrow necks and wider bodies (ink-bottle pores). This type of pores was related to the blockage of the mesoporous channels by large TiO_2 nanocrystals as suggested by the HRTEM image. A high degree of order on the mesoporous length scale was demonstrated by the narrow pore size (2-50 nm) distribution curve (Fig. 5). Based on the BJH method, the estimated corresponding pore size is 4.79 nm. In addition, the BET surface area and total pore volume of the TiO_2 flakes are $125.91\text{ m}^2\text{ g}^{-1}$ and $0.2105\text{ cm}^3\text{ g}^{-1}$, respectively.

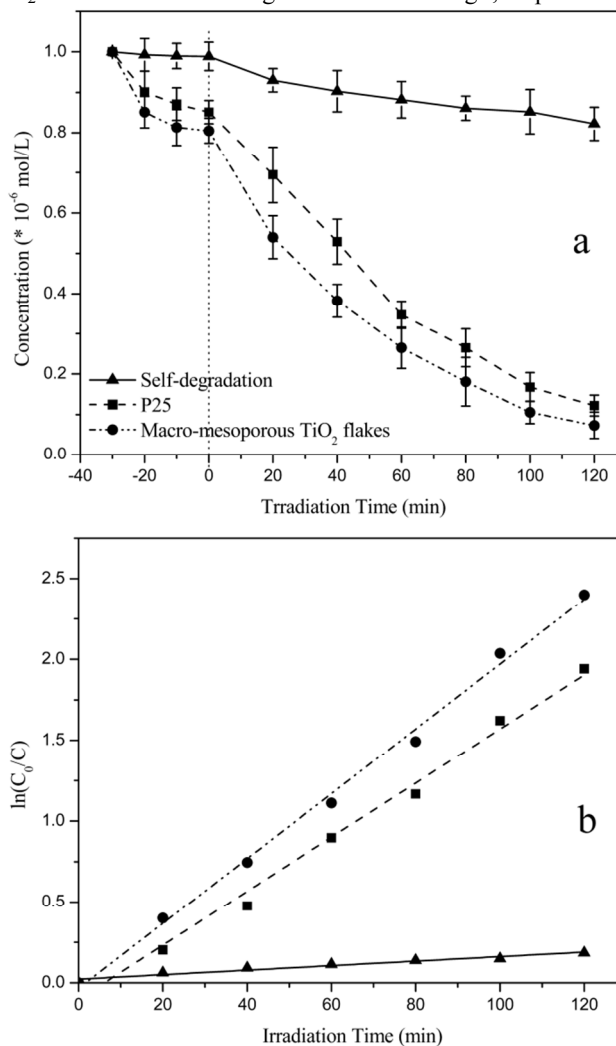


Fig. 6 (a) The residual concentrations of RhB dye solution ($C_0 = 1 \times 10^{-5}\text{ M}$, pH 6.0) after the dark adsorption and UV photodegradation by the TiO_2 flakes and P25. Error bars denote standard deviations of three measurements. And (b) the corresponding plots of $\ln(C_0/C)$ versus the irradiation time, showing the fitting results using the pseudo-first-order reaction.

To demonstrate the potential applicability of the ordered macro-mesoporous TiO_2 flakes for the removal of dye pollutants from wastewater, the photocatalytic activity of the TiO_2 flakes was evaluated by a test reaction of measuring the amount of RhB remaining in solutions in the dark and under UV illumination at regular intervals. For comparison, a

commercially available titania photocatalyst P25 (codoped 70% anatase and 30% rutile TiO₂) was characterized under the same conditions. The dark experiment for 30 min was carried out to determine the photodegradation of RhB without the effect of the adsorption of RhB (Fig. 6a). It was obvious that, most dye molecules (ca. 98.9%) remained in the solution without any photocatalyst after in the dark, whereas a large number of dye molecules were adsorbed on the surface of photocatalysts (ca. 19.5% and ca. 14.9% for TiO₂ flakes and P25, respectively), indicating that the macroporous structure is helpful for improving the photocatalytic performance because of the effective diffusion of dye molecules.³⁹ Then self-degradation of RhB proceeded up to ca. 17.2% after 120 min of UV-light irradiation while degradation of ca. 73.2% and ca. 72.9% are performed by the synthesized TiO₂ flakes and P25, respectively. In Fig. 6b, straight lines are found for all materials, indicating that the degradation of RhB is pseudo-first-order expression, which may be expressed as follows: $\ln(C_0/C) = kt$,³³ where C_0 and C are the initial concentration and the reaction concentration of RhB under UV light irradiation and k is the apparent reaction rate (min⁻¹). Thus the photodegradation apparent reaction rate constant obtained from the slope of the simulated straight line is $2.004 \times 10^{-2} \text{ min}^{-1}$ for the obtained TiO₂ flakes. Correspondingly, the apparent rate constant shares the same sequence with the photocatalytic abilities: the obtained TiO₂ flakes > P25 > self-degradation.

The ultraviolet photodegradation mechanism of RhB by TiO₂ has attracted much attention in the past years.^{40, 41} Building on these foundations, the higher photocatalytic activity of the obtained ordered macro-mesoporous TiO₂ flakes than that of P25 could be explained by the following two aspects: 1) The bimodally ordered macro-mesoporous structures. The macroporous lamellar structure could provide effective light propagation path to increase the efficiency of photoabsorption and improve mass transfer of reactants and products.⁴²⁻⁴⁴ And the stable ordered mesostructures with a large surface area can offer more active adsorption sites and photocatalytic reaction centers, which further improved the photocatalytic activity.³¹ 2) The high crystallinity of anatase phase. The pure anatase TiO₂ has a higher photocatalytic activity than other phase TiO₂,^{24, 25} and higher degree of crystallization means that the number of defects decreases and the recombination of photo-excited electrons and holes could be reduced.⁴³

Conclusions

In summary, a highly ordered macro-mesoporous anatase TiO₂ flakes were successfully prepared by using fresh natural rose petals and triblock copolymer P123 as dual templates in a sol-gel reaction. The fresh natural rose petals with the especial array of micropapillae and the microgrooves were inexpensive, nontoxicity, environment-friendly and widely distributed which can be provided to new macroporous biotemplate and removed

easily. The resulted macro-mesoporous TiO₂ flakes calcined at 450°C for 3 h exhibited slightly higher photocatalytic activity in the photodegradation of RhB in aqueous suspensions than that of the commercial nonporous photocatalyst P25. Thus, it can be concluded that the high photocatalytic activity of the TiO₂ films calcined at 450 °C was related to their highly crystallinity of anatase phase, bimodally ordered macro-mesoporous structures with larger surface area.

Acknowledgements

This research was supported by the Suzhou Science and Technology Project in Jiangsu Province (No. SYG201320).

Notes and references

^a Key Laboratory of Analytical Chemistry for Biology and Medicine, Ministry of Education, College of Chemistry and Molecular Sciences, Wuhan University, Wuhan 430072, People's Republic of China.

^b Suzhou Research Institute of Wuhan University, Suzhou 215123, People's Republic of China.

^c Analytical and Testing Center, Huazhong University of Science and Technology, Wuhan 430074, People's Republic of China.

* Corresponding author: Shaobo Mo (Tel: +8602768764510; Fax: +8602768752136)

** Corresponding author: Hua Tong (E-mail address: sem@whu.edu.cn; Tel: +8602768764510; Fax: +8602768752136)

1. L. J. Lu, F. Teng, SenTapas, D. Y. Qi, L. Z. Wang and J. L. Zhang, *Appl. Catal. B-Environ.*, 2015, **163**, 9-15.
2. Y. Xin, P. Jiang, M. Q. Yu, H. C. Gu, Q. Li and Z. L. Zhang, *J. Mater. Chem. A*, 2014, **2**, 6419-6425.
3. G. Q. Song, Y. X. Lu, Q. Zhang, F. Wang, X. K. Ma, X. F. Huang and Z. H. Zhang, *RSC Adv.*, 2014, **4**, 30221.
4. R. Y. Zhang, D. K. Shen, M. Xu, D. Feng, W. Li, G. F. Zheng, R. C. Che, A. A. Elzatahry and D. Y. Zhao, *Adv. Energy Mater.*, 2014, **4**, 1301725.
5. L. C. Jia, H. Q. Wang, D. Dhawale, C. Anand, M. A. Wahab, Q. M. Ji, K. Ariga and A. Vinu, *Chem. Commun.*, 2014, **50**, 5976-5979.
6. J. Q. Zhao, P. Wan, J. Xiang, T. Tong, L. Dong, Z. N. Gao, X. Y. Shen and H. Tong, *Micropor. Mesopor. Mat.*, 2011, **138**, 200-206.
7. D. M. Antonelli and J. Y. Ying, *Curr. Opin. Colloid In.*, 1996, **1**, 523-529.
8. Z. Y. Yuan and B. L. Su, *J. Mater. Chem.*, 2006, **16**, 663-677.
9. N. D. Petkovich and A. Stein, *Chem. Soc. Rev.*, 2013, **42**, 3721-3739.
10. S. M. Sun, W. Z. Wang and L. Zhang, *J. Mater. Chem.*, 2012, **22**, 19244.
11. Q. Dong, H. L. Su, D. Zhang, Z. T. Liu and Y. J. Lai, *Micropor. Mesopor. Mat.*, 2007, **98**, 344-351.
12. R. Selvakumar, N. Seethalakshmi, P. Thavamani, R. Naidu and M. Megharaj, *RSC Adv.*, 2014, **4**, 52156-52169.
13. Y. Lang, D. P. Finn, F. Caruso and A. Pandit, *RSC Adv.*, 2014, **4**, 44418-44422.
14. I. Guterman, M. Shalit, N. Menda, D. Piestun, M. Dafny-Yelin, G. Shalev, E. Bar, O. Davydov, M. Ovadis and M. Emanuel, *Plant Cell*, 2002, **14**, 2325-2338.

15. L. Feng, Y. N. Zhang, J. M. Xi, Y. Zhu, N. Wang, F. Xia and L. Jiang, *Langmuir*, 2008, **24**, 4114-4119.
16. S. T. Navale, G. D. Khuspe, M. A. Chougule and V. B. Patil, *RSC Adv.*, 2014, **4**, 27998.
17. N. C. Dyck and G. P. Demopoulos, *RSC Adv.*, 2014, **4**, 52694-52701.
18. G. Sahu, S. W. Gordon and M. A. Tarr, *RSC Adv.*, 2012, **2**, 573-582.
19. J. Du, X. Y. Lai, N. L. Yang, J. Zhai, D. Kisailus, F. B. Su, D. Wang and L. Jiang, *ACS Nano*, 2010, **5**, 590-596.
20. M. Motegh, J. R. van Ommen, P. W. Appel and M. T. Kreutzer, *Environ. Sci. Technol.*, 2014, **48**, 1574-1581.
21. L. H. Nguyen, V. Aravindan, S. A. Kulkarni, F. Yanan, R. R. Prabhakar, S. K. Batabyal and S. Madhavi, *ChemElectroChem*, 2014, **1**, 539-543.
22. V. A. Ganesh, A. S. Nair, H. K. Raut, T. M. Walsh and S. Ramakrishna, *RSC Adv.*, 2012, **2**, 2067.
23. K. M. Schindler and M. Kunst, *J. Phys. Chem.*, 1990, **94**, 8222-8226.
24. Y. H. Hsien, C. F. Chang, Y. H. Chen and S. Cheng, *Appl. Catal. B-Environ.*, 2001, **31**, 241-249.
25. Y. H. Zhang, A. Weidenkaff and A. Reller, *Mater. Lett.*, 2002, **54**, 375-381.
26. C. T. Kresge, M. E. Leonowicz, W. J. Roth, J. C. Vartuli and J. S. Beck, *Nature*, 1992, **359**, 710-712.
27. Y. Li, Z. Y. Fu and B. L. Su, *Adv. Funct. Mater.*, 2012, **22**, 4634-4667.
28. L. Ma, M. Liu, T. Y. Peng, K. Fan, L. L. Lu and K. Dai, *Mater. Chem. Phys.*, 2009, **118**, 477-483.
29. S. Netpradit, P. Thiravetyan and S. Towprayoon, *Water Res.*, 2004, **38**, 71-78.
30. P. V. Messina and P. C. Schulz, *J. Colloid Interf. Sci.*, 2006, **299**, 305-320.
31. W. y. Dong, C. W. Lee, X. c. Lu, Y. j. Sun, W. m. Hua, G. s. Zhuang, S. c. Zhang, J. m. Chen, H. q. Hou and D. y. Zhao, *Appl. Catal. B-Environ.*, 2010, **95**, 197-207.
32. Q. Wang, C. C. Chen, D. Zhao, W. H. Ma and J. C. Zhao, *Langmuir*, 2008, **24**, 7338-7345.
33. T. Y. Ma, X. J. Zhang and Z. Y. Yuan, *Micropor. Mesopor. Mat.*, 2009, **123**, 234-242.
34. G. S. Shao, X. J. Zhang and Z. Y. Yuan, *Appl. Catal. B-Environ.*, 2008, **82**, 208-218.
35. T. S. Natarajan, M. Thomas, K. Natarajan, H. C. Bajaj and R. J. Tayade, *Chem. Eng. J.*, 2011, **169**, 126-134.
36. P. C. A. Alberius, K. L. Frindell, R. C. Hayward, E. J. Kramer, G. D. Stucky and B. F. Chmelka, *Chem. Mater.*, 2002, **14**, 3284-3294.
37. U. Balachandran and N. G. Eror, *J. Solid State Chem.*, 1982, **42**, 276-282.
38. R. J. Capwell, F. Spagnolo and M. A. DeSesa, *Appl. Spectrosc.*, 1972, **26**, 537-539.
39. T. Kimura, N. Miyamoto, X. J. Meng, T. Ohji and K. Kato, *Chem. Asian. J.*, 2009, **4**, 1486-1493.
40. J. Zhuang, W. Dai, Q. Tian, Z. Li, L. Xie, J. Wang, P. Liu, X. Shi and D. Wang, *Langmuir*, 2010, **26**, 9686-9694.
41. J. ZHAO, T. WU, K. WU, K. OIKAWA, H. HIDAKA and N. SERPONE, *Environ. Sci. Technol.*, 1998, **32**, 2394-2400.
42. T. V. Teperik, F. J. García de Abajo, A. G. Borisov, M. Abdelsalam, P. N. Bartlett, Y. Sugawara and J. J. Baumberg, *Nat. Photonics*, 2008, **2**, 299-301.
43. X. C. Wang, J. C. Yu, C. M. Ho, Y. D. Hou and X. Z. Fu, *Langmuir*, 2005, **21**, 2552-2559.
44. J. G. Yu, Y. R. Su and B. Cheng, *Adv. Funct. Mater.*, 2007, **17**, 1984-1990.